Deep Silicon Amorphization Induced by Femtosecond Laser Pulses up to the Mid-Infrared

Mario Garcia-Lechuga,* Noemi Casquero, Andong Wang, David Grojo, and Jan Siegel*

Direct laser writing of amorphous lines in crystalline silicon has the potential for becoming a flexible alternative to silicon-on-insulator technology for photonic integrated circuits. Yet, the maximum amorphous layer thickness achieved is 60 nm, which is below the requirements for waveguiding at telecom wavelengths. Here, the authors report on different strategies to push the layer thickness beyond today's limit. To this end, irradiation with femtosecond laser pulses covering an extremely broad wavelength range (515 nm–4 μm) up to the yet unexplored near- and mid-infrared region of silicon transparency is investigated. The results show that much thicker amorphous layers can be obtained upon multipulse irradiation at 3-μm wavelength. The deepest amorphization is achieved in silicon wafers covered with a thick silicon dioxide layer that strongly assists the heat extraction, yielding steep index profiles with a maximum amorphous layer thickness of 128 nm. This superior thickness is compatible with single mode waveguiding for a symmetric waveguide configuration. This study also contributes to a better understanding of the mechanisms involved in laser-induced amorphization.

1. Introduction

Silicon is a key material for the electronics industry, owed mainly to its abundance on earth, its semiconducting properties, and the existence of two structurally different solid phases (crystalline and amorphous) with very different physical properties. The arrival of silicon photonics further expanded the

Dr. M. Garcia-Lechuga,[+] Dr. A. Wang, Dr. D. Grojo
Aix-Marseille Université
CNRS, LP3 UMR 7341, Marseille 13009, France
E-mail: mario.garcialechuga@uam.es
N. Casquero, Dr. J. Siegel
Laser Processing Group
Instituto de Óptica
IO-CSIC
Serrano 121, Madrid 28006, Spain
E-mail: j.siegel@csic.es

[+]Present address: Departamento de Física Aplicada, Universidad Autónoma de Madrid, Campus de Cantoblanco, 28049 Madrid, Spain

outreach of silicon, implemented by coupling silicon chip components to fiber optic telecommunication systems operating typically around 1550 nm, where silicon is transparent.[1,2] However, in order to allow confined light propagation, it was necessary to develop the silicon-on-insulator concept that allows fabrication of optical circuits with lithographic methods similar to those used for electronics systems. This represents a major advantage to capitalize on the huge investment made by the semiconductor industry on these technologies. However, a drawback is the lack of flexibility due to the requirements of expensive mask prefabrication and tedious processing cycles to achieve the desired architectures. It would therefore be highly desirable to develop a versatile direct-write technology for refractive index engineering in Si. While this idea has been implemented successfully by surface amorphization using ion implantation,[3] the approach still required the use of masks to define the waveguide channels. To overcome this limitation, we propose to exploit laser writing of amorphous Si surface structures. This would lead to a very simple way to create an embedded channel of higher refractive index than the crystalline phase constituting a standard Si wafer and therefore provide a unique opportunity for flexible fabrication of structures potentially supporting guided modes on Si wafers. Only recently, reconfigurable switching operations of amorphous Si ridge waveguides on top of crystalline silicon, fabricated by electron beam lithography, have been demonstrated.[4] Making available a laser-based tool for direct writing of embedded waveguides holds great potential for a new booster for the already rapidly growing field of silicon photonics.

The ability of ultrashort pulsed laser irradiation to melt silicon and induce resolidification into either the crystalline or amorphous phase has already been observed in 1979 by the Bloembergen group.[5,6] The experimental parameters that influence the melting and quenching kinetics of the material—and thus the final phase obtained—are the laser wavelength, pulse duration, number of pulses, as well as the crystal orientation. One of the early works that provides quantitative measurements of the layer thickness was reported by Smirl and coworkers, obtaining thickness values of $t \approx 25$ nm by using pulses of 7-ps duration at 1-μm wavelength.[7] The first wavelength dependent thickness-study has been performed by Izawa et al. using femtosecond laser pulses at specific irradiation

wavelengths (267, 400, 800, 1560 nm), yielding a maximum thickness of $t \approx 56$ nm.[8,9] Comparable maximum thickness values were obtained by several other groups: The Bonse group investigated conditions of single, 30 fs laser pulse irradiation at 800 nm, obtaining a maximum thickness of $t \approx 60$ nm.[10–12] Their most recent study[12] on amorphization and recrystallization of bare $Si_{<111>}$ and $Si_{<100>}$ introduces a novel method for determination of the amorphous layer thickness: spectroscopic imaging ellipsometry. This optical method allows high resolution measurements of the lateral thickness profile of amorphous spots. The Siegel group also used fs laser pulses and explored irradiation wavelengths of 400, 800, and 1030 nm, obtaining a maximum thickness value of $t \approx 60$ nm.[13–15] Very recently, Colombier et al. reported a thickness of $t \approx 50$ nm for fs laser irradiation at 800 nm.[16] Gesuele et al. also reported the same thickness value for laser irradiation at 1033 nm with slightly longer pulses (850 fs).[17] One of the very few works on amorphization with mid-infrared (MIR) fs laser pulses is by Werner et al.,[18] who reported a 50 nm layer thickness upon irradiation at 2.75 μm. It should be underlined at this point that in most of the cited works, amorphization was induced by multiple laser pulses, although a dedicated study of the influence of the pulse number has not yet been performed. Moreover, several of these studies reported on the formation of periodic amorphous laser induced periodic surface structures, with a width close to the laser wavelength, a length close to the spot size, and a thickness not exceeding the above mentioned values.[13,15–17,19] It is worth mentioning that the fs laser-induced amorphization process is not accompanied by a change in the surface topography, except the temporary removal of the 2–3 nm thick native oxide layer, as convincingly shown in ref. [12].

In view of the previous works cited, there seems to exist a natural upper limit for the thickness of an amorphous layer that can be formed by ultrafast laser irradiation, at least for the parameter range explored so far in the literature. In order to overcome this limit, we have explored a much wider range of laser wavelengths, ranging from 515 nm up to 4.0 μm, paying particular attention to the infrared region where silicon is transparent (band gap $E_{gap} = 1.12$ eV), in order to attempt triggering deeper amorphization. Moreover, we have systematically investigated the influence of the pulse number and the crystal orientation of Si (<100> and <111>). Additionally, we have investigated the influence of a thick silicon dioxide cover layer on the amorphous layer thickness, since its presence is expected to strongly influence the heat extraction of the deposited laser energy.

2. Results and Discussion

2.1. Surface Amorphization for $\lambda_{laser} = 1.55$ μm

For an efficient exploration of the enormous parameter space and its influence on the thickness of the amorphous layer, it was crucial to employ a quantitative optical diagnostic. To this aim, we have used an optical microscopy system and interpreted interference effects occurring on coherent illumination light reflected at the front and the back surface of the amorphous layer (see also Experimental Section).[11,15] While the thickness of the layer can be rapidly determined with this method even for small laser spots (down to sub-10 μm in our study), the fabrication of written lines, sample cross sections, and inspection by SEM would have required unrealistic resources. In order to verify the validity of the optical method, we have performed a comparative study on irradiations performed for a single material system ($Si_{<111>}$ with native oxide) at a single laser wavelength ($\lambda_{laser} = 1.55$ μm), producing single amorphous spots (for optical analysis) as well as amorphous lines (optical analysis as well as direct SEM images of cross sections). According to Izawa et al.[8] (see Introduction), this irradiation wavelength was leading in their study to the thickest amorphous layers, and therefore provide a good starting point in our quest for ultradeep structuring.

Figure 1a–d shows the results of the optical method in the determination of the layer thickness of an amorphous layer induced by a single laser pulse. The interference nature of the reflectivity images can be clearly appreciated by the fact that the annular intensity distribution changes completely when changing the LED illumination wavelength upon observation of the same amorphous spot. By extracting radial reflectivity profiles of the two imaged spots (cf. Figure 1c), the oscillatory behavior with different periods according to the illumination wavelength can be seen. When moving from outside the spot ($x < -10$ μm) toward the center, the reflectivity at $\lambda_{LED} = 460$ nm rises sharply, reaches a maximum, passes through a local minimum and then rises again to a second local maximum at the spot center ($x = 0$ μm). This evolution is consistent with the calculated behavior shown in Figure 1d and indicates a maximum thickness of about $t = 68$ nm. In comparison, the reflectivity profile at $\lambda_{LED} = 810$ nm in Figure 1c shows a somewhat smoother rise and reaches a maximum at a position located more toward the center, after which it features a decreasing behavior. Comparing this experimental profile with the corresponding calculated curve in Figure 1d, a maximum thickness at the spot center of about $t = 64$ nm is obtained. The thickness values obtained by both illumination wavelengths can be considered as consistent within the experimental error of this method (<10 nm).

Additional experiments were performed for this laser wavelength to fabricate amorphous lines upon sample displacement, using a focal length $f = 150$ mm, and moving the sample at constant speed ($v_{scan} = 2.5$ mm s^{-1}) upon irradiation with a train of laser pulses. The effective incident pulse number N_{eff} on the sample per unit area was controlled via a change of the pulse repetition rate ($f_{rep} = 125, 250, 500, 1000,$ and 2000 Hz), according to $N_{eff} = d_{eff} \cdot f_{rep}/v_{scan}$, where d_{eff} corresponds to the diameter of the amorphous line written, following the method reported in ref. [13]. The optical microscope image of the line that shows highest contrast upon illumination at $\lambda_{LED} = 810$ nm is displayed in Figure 1e. The figure includes the extracted reflectivity profile, showing a stronger modulation than obtained for the amorphous spot and therefore indicating a thicker amorphous layer. By comparison to the calculation in Figure 1d a thickness value of $t = 81$ nm can be estimated.

This value has been confirmed by performing sample cleaving and measuring directly the thickness of the amorphous layer at the line cross section with SEM (JEOL JSM-6500F) using secondary electron detection. This method allowed distinguishing the laser-induced amorphous top layer
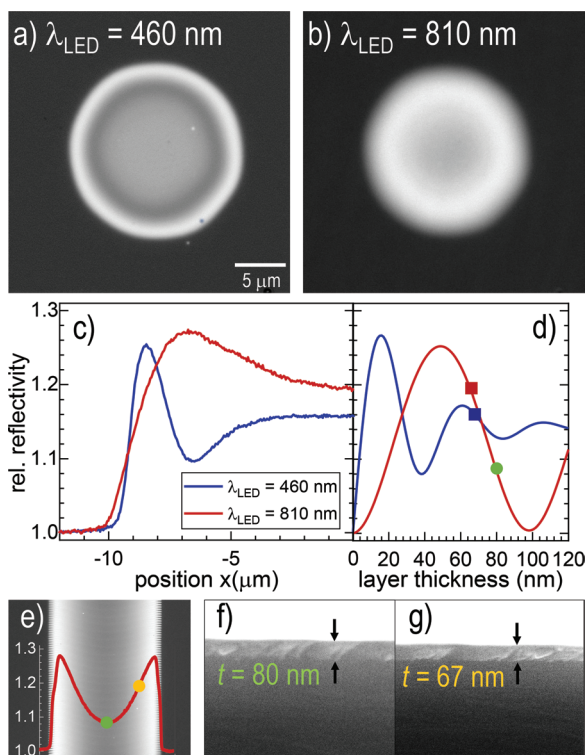
**ADVANCED
SCIENCE NEWS**

www.advancedsciencenews.com

**ADVANCED
OPTICAL
MATERIALS**

www.advopticalmat.de

Figure 1. Femtosecond laser-induced amorphization at λ_{laser} = 1.55 μm on Si$_{<111>}$. a) Optical microscopy image of a region exposed to a single laser pulse (N = 1) at F = 370 mJ cm^{-2}, using LED illumination at λ_{LED} = 460 nm. b) Optical microscopy image of the same region using a different illumination wavelength, λ_{LED} = 810 nm. c) Radial reflectivity profile extracted from images (a) and (b), normalized to the reflectivity of the unmodified regions of the Si sample. d) Calculated normalized reflectivity evolution as a function of thickness of an amorphous top layer on a crystalline substrate, plotted for the two illumination wavelengths employed (see text and Experimental Section). The blue and red symbols correspond to the best match of the corresponding curve values obtained for x = 0 in plot (c). The additional green symbol corresponds to the extracted reflectivity value from (e) (see next). e) Optical microscopy image of a laser-written amorphous line (width = 75 μm) upon sample displacement at constant speed (2.5 mm s^{-1}) and 500 Hz pulse repetition rate (N_{eff} = 15) using a larger focal length (i.e., larger spot size). The inset shows the extracted transversal reflectivity profile at 810 nm wavelength using the same vertical scale as in (c) and (d). The green and yellow symbols mark the positions at which the SEM images of the cleaved cross section shown in (f) and (g) (in-plane perspective of the sample) have been recorded, which show the presence of an amorphous layer with a thickness of t = 80 nm in (f) and t = 67 nm in (g).

from the crystalline bulk material underneath. Figure 1f displays the image obtained in the line center, yielding t = 80 nm, which confirms the value determined optically. Recording an SEM image off-center (Figure 1g), taken at the position of the yellow point in Figure 1e confirms that the thickness decreases toward the line border (t = 67 nm), as expected from a Gaussian intensity distribution of the laser at the sample and in agreement with the reflectivity profile.

The conclusions that can be drawn from this initial study are threefold: First, the optical method can indeed be considered as valid to quantify the thickness of the amorphous layer. Second, the fact that the laser-induced region gives rise to an

optical interference pattern demonstrates that the amorphous–crystalline interface is optically flat. This observation confirms the deterministic homogeneous melting process, as well as an equivalent interfacial solidification mechanism. Third, using laser pulses in the Si transparency regime, the maximum thickness values reported in literature (t_{max} = 60 nm)[11,14] can be overcome already by line writing using near-infrared (NIR) laser pulses in the transparency regime of silicon ($t_{1.55μm}$ = 80 nm). Moreover, another advantage of the optical method is the ability to retrieve from the reflectivity image the thickness profile of the amorphous spot or line. Applied to channel writing for photonic circuits applications, this can provide the exact structure geometry to anticipate by calculations the potential waveguide performances.

2.2. Laser Wavelength Dependence

As a next step, we have explored the laser wavelength-dependence of the layer thickness, spanning a range of λ_{laser} = 515 nm–4 μm. The results for the case of single laser pulses (N = 1) on Si$_{<111>}$ covered by a thin native oxide layer are shown in **Figure 2**. For each wavelength, the amorphous spot obtained at the highest tested pulse fluence below the ablation threshold was analyzed. The discrete energy scanning procedure based on neutral density filters causes that in extreme cases when this value is 15% below the ablation threshold limit. In each case, the optical microscope images (recorded at λ_{LED} = 810 nm) feature a bright annular ring structure and a darker center (cf. Figure 2a–f). This reflectivity distribution is similar to the one observed in Figure 1b and is indicative of a layer thickness $t \gg 50$ nm, at which the calculated reflectivity curve in Figure 1d begins to decrease.

As for Figure 1, the maximum thickness values have been extracted by comparing the experimental reflectivity profiles extracted from Figure 2a–f to the calculated profile at λ_{LED} = 810 nm shown in Figure 1d. We would like to stress that the calculated profile, using a single data for the optical properties did lead to a good match with the experimental reflectivity modulation amplitudes for all laser irradiation wavelengths, (cf. Experimental Section). This fact strongly indicates that the structural state of the amorphous phase produced by ultrashort laser pulses of different laser wavelengths is similar.

Figure 2g displays the maximum thickness values obtained in the spot center as a function of laser wavelength, extracted from the images shown in Figure 2a–f. The behavior shows a general increase toward longer wavelengths, except for the shortest wavelength that obtains an equally high value as for the longest wavelengths. This result demonstrates that the trend does not follow the expected monotonous evolution with laser wavelength, corresponding to the transition from linear absorption (λ_{laser} = 515 nm) to multiphoton absorption ($\lambda_{laser} \geq 1.03$ μm). Intuitively, one might expect that the increase in the optical penetration depth (OPD) with laser wavelength should lead to a corresponding increase in melt depth and thus amorphization depth. However, when calculating the OPD for linear absorption of c-Si (OPD$_{515nm}$ = 980 nm) it becomes evident that even for this short wavelength, the OPD value is much larger than the value obtained for the amorphous
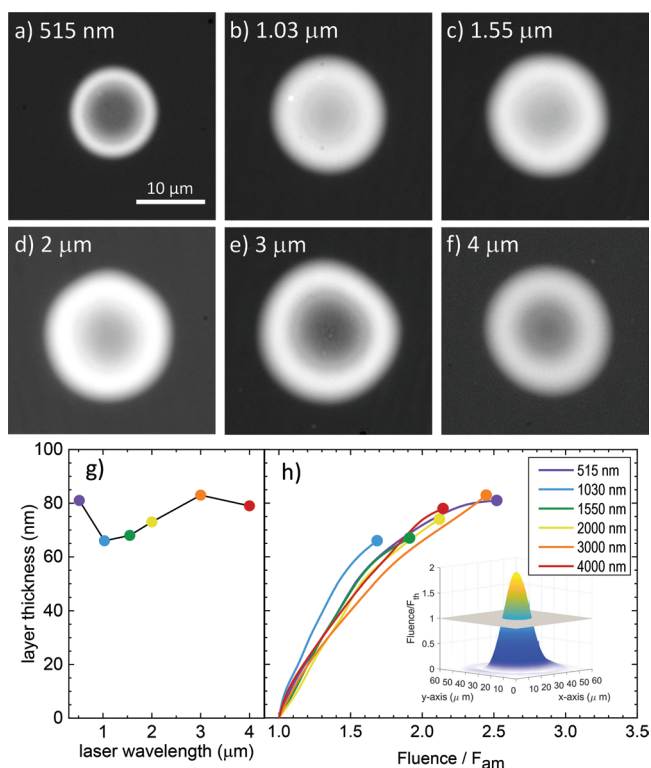
**ADVANCED
SCIENCE NEWS**

www.advancedsciencenews.com

**ADVANCED
OPTICAL
MATERIALS**

www.advopticalmat.de

Figure 2. Laser-induced amorphization of $Si_{<111>}$ for different laser wavelengths λ_{laser} (see labels). a–f) Upper frames: Optical microscope images recorded at λ_{LED} = 810 nm, corresponding to single pulse irradiations (N = 1) performed at the highest fluence below the ablation threshold (F_{515nm} = 250 mJ cm^{-2}, $F_{1.03\mu m}$ = 320 mJ cm^{-2}, $F_{1.55\mu m}$ = 370 mJ cm^{-2}, $F_{2\mu m}$ = 390 mJ cm^{-2}, $F_{3\mu m}$ = 510 mJ cm^{-2}, $F_{4\mu m}$ = 730 mJ cm^{-2}). The image contrast is set to [0.95, 1.30]. g) Layer thickness in the spot center as a function of laser wavelength, determined using the reflectivity calculation shown in Figure 1d. h) Evolution of the position-dependent layer thickness as a function of the local laser fluence, normalized to the individual amorphization threshold fluence (see text for details). The inset shows the spatial fluence distribution at the sample position for λ_{laser} = 1.55 μm and $F_{1.55\mu m}$ = 370 mJ cm^{-2}, determined by using a calibrated infrared microscopy system.

layer thickness (t_{515nm} = 81 nm). Taking this large difference into account, two possible scenarios can be sketched for λ_{laser} = 515 nm. The first scenario assumes that the initial melt depth is comparable to the corresponding OPD_{515nm} value and amorphization only occurs during the final stage of the solidification process. This scenario is highly unlikely since the thermal gradient is highest immediately after energy deposition. The second scenario assumes that the initial melt depth is comparable to the t_{515nm} value, shortened by an additional contribution of two-photon absorption. Such behavior is likely to occur, taking into account that strong two-photon absorption contribution has been demonstrated for above band gap excitation of Si at 620 nm (OPD_{620nm} = 2930 nm).[20,21] Lipp et al. have modeled the melting of c-Si with above-band gap NIR pulses (800 nm, 130 fs) and predict melt depth of ≈160 nm for fluences close to the ablation threshold.[22] This value is a factor of two to three higher than the thickness of an amorphous layer observed experimentally under similar conditions,[11,14] but considerably smaller than the OPD (OPD_{800nm} ≈ 10 μm). It is

worth noting that Si has an indirect band gap (E_{gap} = 1.12 eV), which implies that a transition requires phonon assistance for momentum conservation. State and band filling, as well as band gap shrinkage may influence the excitation process but have reported to be of minor importance at least for excitation above band gap.[21]

In order to quantify the amorphous layer thickness not only at the spot center but as a function of the lateral position, we have performed a detailed analysis of the images taking into account the equivalent Gaussian spatial intensity distribution of the laser light at the sample plane. This distribution has been measured experimentally (see Experimental Section) for each wavelength, which allowed us to assign to each spatial position x of a given reflectivity image a corresponding local fluence value $F(x)$. The local fluence values were normalized to the threshold fluence value for amorphization (F_{am}), determined by the local fluence/position at which the reflectivity begins to increase. These normalized local fluence values F/F_{am} were used as the abscissa of the plot shown in Figure 2h. The ordinate of the plot corresponds to the layer thickness, t, at each local fluence F/F_{am} and the data points have been obtained by correlating the extracted experimental reflectivity profiles extracted from the images (not shown) and the calculated evolution shown in Figure 1d. This method of normalization and representation has the advantage that irradiation parameter-dependent differences for different laser wavelengths, such as beam waist and amorphization threshold, can be eliminated in order to allow for a better comparison of the intensity-dependent amorphization behavior for different wavelengths. It should be mentioned that this representation is based on the hypothesis of a pure local fluence response of the material, that is, lateral energy transport as electron or heat diffusion can be excluded. Such hypothesis is reasonable in view of the large amorphous spot diameters (10 μm or larger) compared to the thickness of the amorphous layer (80 nm maximum), yielding a size ratio in excess of 1:100.

The obtained behavior shown in Figure 2h features initially an almost linear increase of the thickness with fluence for all wavelengths, consistent with a linear increase of the melt depth accompanied by rapid quenching. At a thickness of t = 30 nm, the increase is slowed down for all wavelengths, causing a curve bending for higher fluences. While the slopes of this initial increase show slight differences, they do not follow a clear order in terms of wavelength, as might be expected if the thickness was determined by a transition from linear absorption to multiphoton absorption, which would classify λ_{laser} = 515 nm and 1.03 μm to be dominated by one-photon absorption, λ_{laser} = 1.55 and 2.0 μm by two-photon absorption, λ_{laser} = 3.0 μm by three-photon absorption, and λ_{laser} = 4.0 μm by four-photon absorption.

The two wavelength values for which the deepest amorphization can be achieved are λ_{laser} = 515 nm and 3.0 μm, although the shape of the curves in Figure 2h are completely different. For λ_{laser} = 515 nm, the thickness evolution upon fluence increase shows signs of saturation, which suggests that the potential of this wavelength for deeper amorphization is small. In contrast, no signs of saturation are observed for λ_{laser} = 3 μm, or other wavelengths in the NIR and MIR,

**ADVANCED
SCIENCE NEWS**

www.advancedsciencenews.com

**ADVANCED
OPTICAL
MATERIALS**

www.advopticalmat.de

only being limited by ablation. This suggests that higher thickness values should in principle be achievable by exploring other parameters, such as the number of incident laser pulses or the presence of a cover layer for enhanced energy dissipation and/or potential increase of the ablation limit.

2.3. Pulse Number Dependence

The influence of the pulse number on the amorphous layer thickness was studied for all wavelengths and pulse fluences. Overall, incubation effects[23] lead to lower ablation thresholds and so the study could not be conducted at the fluence values identified as optimum for the single pulse study in Section 2.2. Therefore, we have limited, where possible, our analysis to fluences, at which the samples could withstand irradiation with at least $N = 5$ without experiencing ablation.

The pronounced effect of multiple pulse irradiation is illustrated in **Figure 3**a–d for the case of $\lambda_{laser} = 3$ μm, showing a considerable darkening in the spot center upon pulse number increase, as a consequence of a thickness increase of the amorphous surface layer (cf. calculation in Figure 1d) along with a moderate increase of the amorphized surface area (due to incubation). Moreover, a pronounced sharpening of the lateral border between the amorphous spot and the
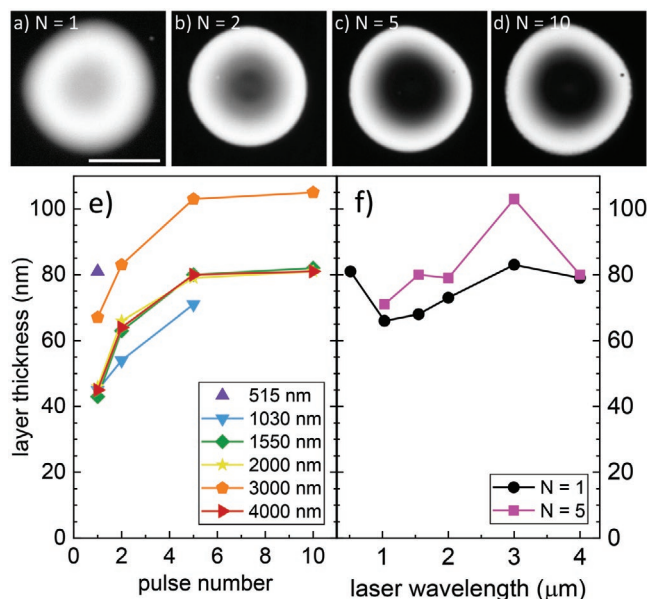
crystalline surrounding can be observed. This behavior indicates a steeper index profile in the phase transition region, which is very relevant for technological considerations as it provides a possibility to control the profile of the written waveguides.

Figure 3e shows the evolution of the extracted maximum layer thickness in the spot center as a function of pulse number for all λ_{laser} studied. The general trend is an increase of the thickness upon multiple pulse irradiations that can be observed also for the other laser wavelengths. The behavior seems intuitive and simple to explain, but is actually rather complex. It has to be considered for this experiment that amorphization cannot be an additive process, in which subsequent pulses further increase the amorphous layer thickness, because each subsequent pulse melts again the entire amorphous layer, plus a certain thickness of the underlying crystalline silicon. The most likely reason for a thickness increase, despite complete melting, is related to the fact that each subsequent pulse "sees" a different material, since the absorption profile is strongly influenced by the presence and thickness of the amorphous layer formed after the previous pulse. This modified absorption profile leads to a modified thickness of the molten layer, which is in general larger because the amorphous phase has a higher absorption coefficient than the crystalline phase for most wavelengths. We attribute the increase in amorphous layer thickness with pulse number to this modification of the molten layer thickness.

Interestingly, near-to saturation is achieved already after few pulses ($N = 5$) and virtually no further thickness increase is observed at $N = 10$, which has a practical aspect of requiring only few pulses for inducing the maximum thickness achievable. A comparison of the multiple-pulse data ($N = 5$) to the single-pulse data is shown Figure 3f. The behavior of the maximum thickness with laser wavelength for $N = 5$ is relatively similar to the one observed for single pulse data. However, a much larger thickness value is achieved for multiple pulse data for $\lambda_{laser} = 3$ μm, with the largest value achieved being $t_{3μm} = 103$ nm, which is 24% larger than for single pulse irradiation at the same wavelength and respective optimum fluence (value quoted in Figure 2h).

Providing an explanation for our experimental observation of an enhanced amorphization thickness at 3 μm wavelength (both for single and multiple pulse irradiations [cf. Figure 3f]) is challenging. In view of the fact that the pulse durations for all wavelength used are comparable, the underlying origin is most likely related to the different absorption depth profiles. Some insight in the absorption mechanisms of NIR and MIR ultrashort laser pulses has been given recently in the theoretical study by E. Petrakakis et al.,[24] who explored a wavelength range of $\lambda_{laser} = 2.2$–3.3 μm. The authors observed that the Kerr effect is important at lower wavelengths, leading to large deviations in the maximum lattice temperature reached, which in turn affects the damage threshold. The authors predict a related non-linear increase of the damage threshold with laser wavelength by ≈50%. Such a threshold increase can be related to our study, since the maximum amorphous layer thickness in Si$_{<111>}$ is observed for the highest fluence just below the damage threshold. In particular, the corresponding fluences for the irradiation wavelengths $\lambda_{laser} = 2$ μm and

Figure 3. Influence of the pulse number, N, on the thickness of the amorphous surface layer formed in Si$_{<111>}$ covered with native oxide. a–d) Optical microscope images recorded with $\lambda_{LED} = 810$ nm, after irradiation at $\lambda_{laser} = 3$ μm with different pulse numbers N (see labels) at $F_{3μm} = 360$ mJ cm^{-2}. The scale bar length in (a) corresponds to 10 μm. e) Thickness in the spot center as a function of pulse number for different laser wavelengths λ_{laser} (see labels), using fluence values at which the sample could withstand at least up to $N = 5$ pulses without ablation (except $\lambda_{laser} = 515$ nm for which even the lowest pulse fluence available was too high to withstand $N = 5$): $F_{515nm} = 250$ mJ cm^{-2}, $F_{1.03μm} = 230$ mJ cm^{-2}, $F_{1.55μm} = 280$ mJ cm^{-2}, $F_{2μm} = 285$ mJ cm^{-2}, $F_{3μm} = 440$ mJ cm^{-2}, $F_{4μm} = 460$ mJ cm^{-2}. f) Thickness in the spot center as a function of laser wavelength for $N = 5$ (fluence values above) compared to $N = 1$ (fluence values from Figure 2).

λ_{laser} = 3 µm with pulse durations used in our study (180 fs) can be compared to those reported by Petrakakis et al. Our experimental data show an ablation threshold increase of 54% ($F_{2µm}$ = 285 mJ cm^{-2}, $F_{3µm}$ = 440 mJ cm^{-2} [see Figure 3e,f]), which is fully consistent with the predicted increase of ≈50% from 2.2 to 3.3 µm.[24]

While this good match of our data with theory provides possible explanation for our observed increase in amorphization thickness upon irradiation at λ_{laser} = 3 µm compared to shorter wavelengths, the observed thickness decrease at λ_{laser} = 4 µm requires further explanation. It should be reminded at this point, that the energy deposition is not the sole factor that determines the thickness of the amorphized layer, but the velocity of the solidification front also plays a key role. Its importance will be demonstrated and discussed in detail in next Section 2.4. In this context, we attribute the decrease of maximum amorphization thickness at 4 µm to a reduced solidification speed within the laser-melted volume, most likely caused by a further enlarged melt depth at λ_{laser} = 4 µm and thus reduced thermal gradients.

2.4. Dependence on Crystal Orientation and Presence of a Thick SiO$_2$ Cover Layer Thickness

While the parameters explored in the previous sections concern laser irradiation (pulse number, energy, and wavelength), the material system itself also offers room for optimization of the thickness of the amorphous layer formed. One important parameter is the crystal orientation, since crystal growth from the melt in Si along the close packed <100> direction has been shown to be faster than along the <111> direction, as a direct consequence of the anisotropic accommodation probability for atoms in the growing phase.[25] Experimentally, this orientation-dependence of the critical velocity for amorphization to occur has been confirmed upon nanosecond laser melting, yielding 14 m s^{-1} for Si$_{<111>}$ and 18 m s^{-1} for Si$_{<100>}$.[26,27] Recent studies using fs laser pulses confirmed the increased difficulty of Si$_{<100>}$ to amorphize.[12,28] Moreover, Yater and coworkers reported an orientation dependence of the maximum amorphous layer thickness achieved using UV nanosecond laser pulses, yielding thicker layers for Si$_{<111>}$.[29]

These studies imply that an even stronger undercooling (and thus larger thermal gradient) is required for surface amorphization in Si$_{<100>}$. Since our study employs much shorter pulses than in the works cited above, a stronger undercooling is expected and amorphization should in principle be straightforward. We have performed the full study reported above (exploring the influence of the pulse number and the laser wavelength) to the case of Si$_{<100>}$. Despite the strong undercooling expected, for certain wavelengths (λ_{laser} = 1.03 and 1.55 µm) single pulse irradiation only led to insignificant amorphization, and that at least N = 2 were necessary to form an amorphous layer thickness t > 40 nm (data not shown). The same inability of strong single pulse amorphization in Si$_{<100>}$ has been reported for λ_{laser} = 800 nm.[14,12] This result underlines the importance of the laser wavelength for the initial energy deposition profile and suggests that these relatively standard wavelengths for fs lasers are not ideal for deep amor-
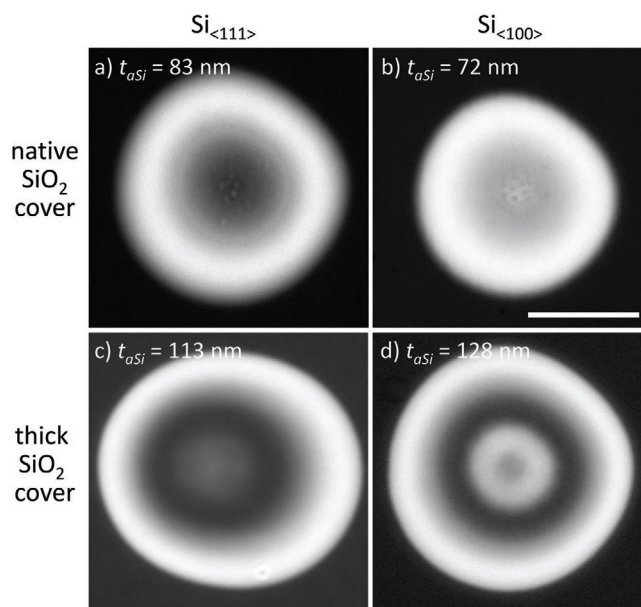

Figure 4. Influence of the crystal orientation and cover SiO$_2$ layer thickness on the thickness of the amorphous surface layer formed (see labels) in Si after irradiation with single laser pulses at λ_{laser} = 3 µm. a–d) Optical microscope images recorded with λ_{LED} = 810 nm for optimized peak fluences $F_{Si<111>nativeSiO2}$ = 510 mJ cm^{-2} (a), $F_{Si<100>nativeSiO2}$ = 440 mJ cm^{-2} (b), $F_{Si<111>thickSiO2}$ = 550 mJ cm^{-2} (c), $F_{Si<100>thickSiO2}$ = 510 mJ cm^{-2} (d). The scale bar length in (b) corresponds to 10 µm. For (a), (c), and (d), the fluences correspond to the highest ones below the corresponding ablation thresholds, except for (b) for which recrystallization was the limiting factor.

phization. Concerning the other wavelengths used in our study, we have found that the maximum thickness was obtained for λ_{laser} = 3 µm, just as for our experiments in Si$_{<111>}$. The comparison of the results obtained in the two sample types is shown in **Figure 4**a,b, yielding a slightly lower value for Si$_{<100>}$ (t = 72 nm) than for Si$_{<111>}$ (t = 83 nm), in agreement with the ns laser results reported in ref. [29].

In view of the importance of heat extraction, we have designed a sample configuration with a thick SiO$_2$ cover layer, in which additional heat extraction is provided in the opposite direction, toward the incident laser beam. It should be mentioned here that a wavelength-dependent reflectivity modulation, caused by interference of the reflections at the front and backside of this layer, may lead to a wavelength-dependent absorption of laser energy in the Si substrate. However, this effect is already considered and taken care of by our experimental method to perform irradiations over a broad range of pulse energies and selecting the one that features the deepest amorphization. Moreover, relating the corresponding fluence to the respective amorphization threshold ensures an automatic relative fluence scaling (see for instance representation in Figure 2h). In terms of heat flow, the thick cover layer acts as an additional heat sink (thermal diffusivity D ≈ 0.008 cm^2 s^{-1}) considerably enhancing melt quenching, which is not the case for a thin native oxide layer. The heat diffusion into the cover layer is initially fast due to the strong thermal gradient imprinted after laser-induced melting. The relevant time scale
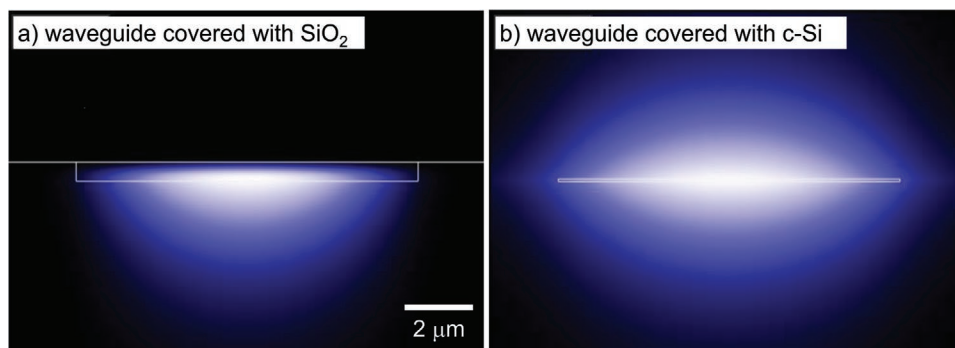
**ADVANCED
SCIENCE NEWS**
www.advancedsciencenews.com

**ADVANCED
OPTICAL
MATERIALS**
www.advopticalmat.de

Figure 5. Calculated mode profile cross sections at a wavelength of 1550 nm for different amorphous Si waveguide configurations using the EIMS 2-D multilayer waveguide mode solver available at ref. [32]. a) Asymmetric waveguide composed of an amorphous Si waveguide (white rectangle) at the surface of crystalline Si covered with a thick SiO_2 layer. b) Symmetric waveguide composed of an amorphous Si waveguide (white rectangle) at the surface of crystalline Si covered with a thick c-Si layer. In both cases, the modes are calculated for the minimum thickness for single mode operation (t_{min} = 560 nm for (a) and t_{min} = 80 nm for (b)). The intensity scale corresponds to the square of the electric field of the TE_{00} mode.

for influencing the amorphization process is the melt duration, which is in the order of t_{melt} = 10 ns.[30] The thermal diffusion length L_{th} can be estimated as $L_{th} \approx (D_{SiO2} \cdot t_{melt})^{1/2}$, yielding L_{th} = 90 nm, which is considerably smaller than the cover layer thickness. Consequently, the cover layer used in our study can be considered as thermally thick.

Figure 4c,d shows the optimized results obtained for single pulse irradiation at the most efficient laser wavelength identified (λ_{laser} = 3 µm). For both crystal orientations, a significant increase of the amorphous layer thickness is observed compared to the samples covered with native oxide. This result confirms our hypothesis that additional heat extraction is beneficial for the formation of thicker amorphous layers. Surprisingly, the <100> crystal orientation, which is less beneficial for amorphization, leads in this configuration to a larger thickness value ($t_{Si<100>SiO2}$ = 128 nm) than for the <111> orientation ($t_{Si<100>SiO2}$ = 113 nm). This might be caused by the complexity of the solidification mechanisms involved, but also a consequence of the discretization of the fluence values used. Moreover, no thickness increase of the amorphous layer upon irradiation with multiple pulses was observed, as opposed to what is observed for $Si_{<111>}$ with native cover layer irradiated at λ_{laser} = 3 µm (see Figure 3f). The important point is that, for both samples with a thick cover layer, irradiated at λ_{laser} = 3 µm, thickness values obtained are almost twice as large as those reported to date (t = 60 nm),[11,14] showing the relevance of the identified optimization parameters. Changing the cover layer thickness toward lower values, in the order of L_{th}, would effectively allow tuning the heat extraction and therefore the phase transformation dynamics,[31] offering in our case a further method to tune the thickness of the amorphous layer.

2.5. Potential for Optical Waveguide Writing

Concerning applications in silicon photonics, particularly optical waveguiding, the largest thickness value achieved in our study is t = 128 nm, using single pulses at λ_{laser} = 3 µm on $Si_{<100>}$ samples covered with a thick SiO_2. While being more than twice as large as previously reported in literature (t = 60 nm in refs. [11,14]), it is insufficient for surface waveguide

applications at telecom wavelengths in this sample configuration. The minimum thickness required for single mode operation has been calculated for an amorphous line written at the surface of crystalline wafer covered with a thick SiO_2 layer. The results are shown in **Figure 5**a for a 10 µm wide waveguide, yielding a minimum thickness for single mode operation of t_{min} = 560 nm, much larger than what has been achieved in the present study.

One reason for the large thickness values required is the configuration of an asymmetric index profile, with a low index cover layer and a high index substrate. If a symmetric index configuration could be achieved, for instance by writing an amorphous line on bare silicon and then depositing a silicon layer on top, the waveguide solver predicts single mode operation for a thickness value t_{min} = 80 nm as shown in Figure 5b, which is accessible by the irradiation strategies presented here (cf. Figures 1f and 3f). We would like to stress, though, that other irradiation parameters are still to be explored, for instance the pulse duration,[33] which might have the potential to increase the amorphous layer thickness beyond current limits, but would require an additional optical arrangement in form of a pulse stretcher for each wavelength to concentrate future works on this question.

3. Conclusions

Surface amorphization of silicon by femtosecond laser pulses is governed by a large number of correlated experimental parameters. In our study, we have explored a large parameter space (laser wavelength, pulse number, pulse energy, Si lattice orientation, introduction of a dielectric cover layer), aimed at maximizing the layer thickness. One of the key findings is that the previously unexplored near- and mid-infrared region of silicon transparency holds promise for deep amorphization, reaching largest thickness values for a laser wavelength of λ_{laser} = 3 µm. We have also confirmed for a wide spectral range of femtosecond laser pulses the strong influence of the crystal orientation reported previously for few wavelengths using nanosecond and femtosecond laser pulses, with $Si_{<111>}$ strongly favoring single pulse amorphization and yielding larger thickness

values. Moreover, the influence of the pulse number on the maximum thickness achieved in $Si_{<111>}$ is found to be related to the pulse fluence, in a sense that a low pulse number can be compensated in part by a fluence increase. Yet, for the specific case of $\lambda_{laser} = 3 \ \mu m$, multipulse irradiation led to the highest thickness value reported to date for bare silicon, $t = 103$ nm. Additionally, multipulse irradiation is beneficial for triggering a sharp index gradient between amorphous and crystalline regions. While the demonstrated influence of number of pulses and crystal orientation is important, we found that the wavelength and the cover layer are two main drivers for achieving deep amorphization. Introducing a thick SiO_2 cover layer as an additional heat sink is found to strongly contribute to amorphization, yielding thickness values not achievable in Si with only a thin native oxide layer. The largest thickness value achieved in our multiparametric study is $t = 128$ nm, using laser pulses at $\lambda_{laser} = 3 \ \mu m$ on Si covered with a micrometer-thick SiO_2 layer. Despite being two times thicker than previously achieved, it is still insufficient for asymmetric surface waveguides operating at telecom wavelengths. We propose the deposition or bonding of a Si cover layer after waveguide writing, which should allow single mode operation for the thickness values achieved in the present study.

Our study has also led to a number of conclusions about the mechanisms involved in laser-induced amorphization. First, the fact that the laser-induced region gives rise to an optical interference pattern for the entire wavelength range studied, demonstrates that in all cases the amorphous–crystalline interface is optically flat. This observation confirms the deterministic homogeneous melting process and suggests an equivalent interfacial solidification mechanism even in the NIR and MIR region. Second, the fact that this optical response can be modeled with a single data set of optical properties of the amorphous phase indicates that the structural state of the amorphous phase produced by ultrashort laser pulses of different wavelengths is similar. Third, the absence of a systematic trend of the evolution of layer thickness versus local fluence for different laser wavelengths demonstrates that the laser absorption cannot be described by a simple model based on single and multiphoton absorption. Fourth, the observed thickness increase with pulse number can be attributed to the modification of absorption profile by the previous pulse, which leads to a modified thickness of the molten layer by the next pulse. Fifth and last, our observation of an optimum wavelength ($\lambda_{laser} = 3 \ \mu m$) for deep amorphization is consistent with a theoretically predicted ablation threshold increase compared to lower wavelengths and reduced thermals gradients/solidification speeds for longer wavelengths. We believe that time-resolved studies of laser-induced amorphization, particularly in the NIR and MIR range have the potential to further contribute to the understanding of the underlying mechanisms and aid to further increase the amorphization depths.

4. Experimental Section

A state-of-the-art ultrafast laser system was used to pump harmonic generators or an optical parametric amplifier so that broadband wavelength tunability from 515 nm to 4 μm becomes accessible for

Table 1. Experimental irradiation conditions for the different wavelengths. f corresponds to the nominal focal length, ϕ_{ap} to the diameter of the aperture used before the lens, P_T to the power transfer through the aperture, w_0 to the beam waist obtained after applying Liu's methodology[35] to the data. η_F is the corresponding correction factor to account for the Airy shape of the beam for fluence determination.[34] The considered energies for analyses do not exceed four times the energy threshold of amorphization.

λ [nm]	f [mm]	ϕ_{ap} [mm]	P_T [%]	w_0 [μm]	η_F
515	50	3.5	76	10.6	0.99
1030	50	4.5	71	17.9	0.99
1550	25	3.0	33	16.8	0.93
2000	25	4.0	33	14.9	0.93
3000	25	5.0	28	15.8	0.93
4000	25	6.5	60	15.7	0.96

the investigations. The Si samples were systemically irradiated with pulses of 180 ± 20 fs as confirmed by autocorrelation measurements at different wavelengths. Six different laser wavelengths were selected for the experiment ($\lambda_{laser} = 515$ nm, 1.03, 1.55, 2.0, 3.0, and 4.0 μm). The irradiation setup included a filtering aperture (diameter $\phi_{ap} = 3.0–6.5$ mm, depending on the wavelength used) before a focusing lens ($f = 50$ mm for $\lambda_{laser} = 515$ nm, 1.03 μm and $f = 25$ mm for the other wavelengths) for precise determination of the local fluence on target, independent of the beam quality. The specific values used are listed in **Table 1** and the details on the metrology aspects can be found in ref. [34].

The sample holder was mounted on XYZ motorized stages. An in situ microscope was installed at ≈45° angle of observation for precise sample positioning and focal plane control, as used in ref. [36]. The pulse energy was controlled by employing reflective neutral density filters, which allowed the authors to perform experiments over a broad range of different (discrete) energy values, measured using a sensitive powermeter (3A, Ophir). The pulse energy values E were converted into peak fluence values F, using the widely used method by Liu[35] with the introduction of a fluence correction factor (η_F) accounting the diffractive effect due to pinhole truncation.[34] Specifically, for each laser wavelength a series of single pulse irradiation at increasing pulse energies was performed from below the amorphization threshold until two to three times the ablation threshold. The beam diameter (at $1/e^2$) $2w_0$ of the equivalent Gaussian profile was obtained by representing the spot diameters as a function of pulse energy, yielding the relation $F = 2 \cdot E \cdot \eta_F / (\pi \cdot w_0^2)$.[34] For the specific case of $\lambda_{laser} = 1.55$ μm, the intensity distribution at the focal position was characterized with an imaging system composed of a microscope objective (100×, NA 0.5, Mitutoyo), a tube lens, and an InGaAs camera (Raptor OWL 640). The acquired 16-bit image, $I_{i,j}$ (a.u.), was translated into an absolute fluence distribution, $F_{i,j}$ (J cm^{-2}), for a given incident energy, thanks to the linear response of the sensor and a calibration procedure.

The samples used for the laser irradiation experiments were commercial crystalline Si wafers with two different orientations (<100> and <111>) covered either by a thin layer of native oxide ($d_{SiO2} = 3$ nm) or by thick layer of SiO_2. The exact sample specifications were as follows: $Si_{<100>nativeSiO2}$ from Siltronix, 1 mm thickness, intrinsic, 200–600 Ωcm, double side polished. $Si_{<111>nativeSiO2}$ from IETM, 0.53 mm thickness, n-doping, 0.002–0.005 Ωcm, single side polished. $Si_{<100>thickSiO2}$ from Siegert, 0.53 mm thickness, p-doping, 1–100 Ωcm, single side polished, $d_{SiO2} = 3.506$ μm. $Si_{<111>thickSiO2}$ from Microchemicals, 0.53 mm thickness, n-doping, 1–10 Ωcm, single side polished, $d_{SiO2} = 1.065$ μm. The d_{SiO2} values were measured with spectroscopic ellipsometry.

A possible laser absorption in the cover layer could be neglected, since SiO_2 features negligible absorption for the spectral window of the laser wavelengths used in this study. There were important challenges in exploring the wide parameter space imposed for this work. It required a multidimensional study of six laser wavelengths and four samples types as a function of pulse number and fluence. In order to keep the number

2100400 (8 of 10)

Table 2. Optical constants of the amorphous and crystalline phase of silicon at the wavelengths used for calculations of the amorphous layer thickness and waveguide mode profiles.[38]

Material	Wavelength	Refractive index [$n + ik$]	
	[nm]	n	k
c-Si	460	4.583	0.130
	810	3.686	0.006
	1550	3.476	0.000
a-Si	460	5.090	1.173
	810	4.110	0.020
	1550	3.538	0.003

of experiments and subsequent analyses to a reasonable (yet still high) level, the pulse number was limited to N = 1, 2, 5, and 10 and the fluence values limited to those accessible directly by the combination of the different attenuation filters. Moreover, for each pulse fluence and pulse number value, a total of three irradiations were performed and analyzed in order to verify the reproducibility.

Characterization of the laser-irradiated samples was performed with an optical microscope in reflection, using monochromatic illumination sources at different wavelengths. This method was frequently used for assessing the thickness of the amorphous layer formed in silicon,[11,15] since its presence led to the appearance of interference fringes in the microscope image, caused by the interference of light reflected at the sample surface with light reflected at the embedded amorphous/crystalline interface. The number of interference fringes was a direct measure of the layer thickness. The microscope used was a Nikon Eclipse Ti equipped with a 100×, 0.9 N.A. objective lens, and a 12 bit CCD camera, employing switchable LED illumination at λ_{LED} = 460 and 810 nm wavelengths.

The modeling for determining the thickness of the amorphous layer was performed with a program using Fresnel equations and based on an exact mathematical description of the interaction of an electromagnetic wave with an isotropic planar multilayered system, normally referred to as Abeles' theory.[37] Each layer was computed to have a given thickness and optical properties (refractive index and absorption coefficients). The program transformed layer by layer in steps of 1 nm the optical constants of c-Si into those of a-Si and calculated the reflectivity of the whole system at the illumination wavelengths as a function of the transformation depth, as already reported in ref. [15]. The optical constants at the wavelengths used by the LED illumination are listed in **Table 2** and were taken from ref. [38].

It should be noted here that there were several publications with tabulated data values for the refractive index and absorption coefficients of the amorphous phase of silicon that differ considerably. The underlying reason was that the atomic structure of the amorphous phase was not as well-defined as the crystalline state was, but depended strongly on the preparation conditions, that is, if it was prepared by ion implantation, thin film growth (depending also on the growth technique), or laser amorphization. In order to evaluate the importance of these differences, the authors calculated the expected reflectivity change upon amorphization using the refractive index and absorption coefficients of several data bases. The results were found to be very robust in terms of the thickness at which reflectivity maxima and minima were produced, yielding thickness variations between data bases of less than 5%. However, considerable changes in the amplitude of the reflectivity modulation were observed for different data sets. This led the authors to choose the tabulated data listed in ref. [38], which best described the experimentally observed modulation amplitudes for all laser wavelengths at the microscope illumination wavelengths 460 and 810 nm, as shown in Figure 1c,d. This could also be appreciated in **Figure 6**, which compared the experimental and calculated maximum reflectivity modulation amplitudes (increase of the relative reflectivity up to the first maximum). For all irradiation wavelengths the experimental values showed only small deviations from the values calculated with
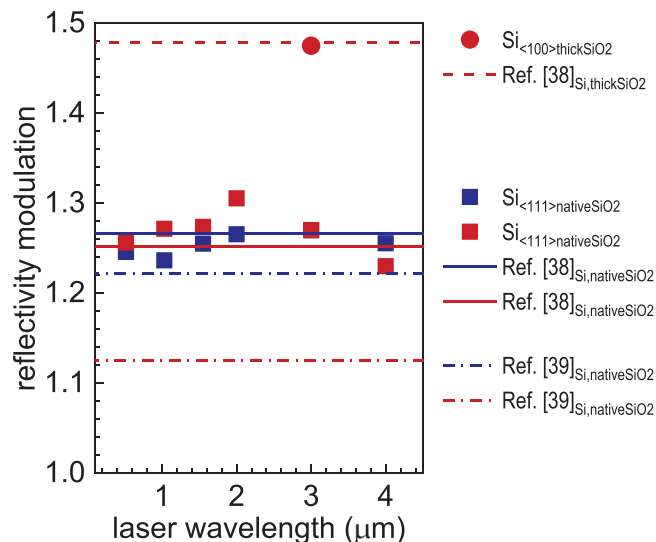

Figure 6. Comparison of the experimental and calculated maximum reflectivity modulation amplitudes for all irradiation wavelength in Si$_{<111>}$ with a native SiO$_2$ layer and for irradiation at 3 μm in Si$_{<100>}$ with a thick SiO$_2$ layer. Blue colored symbols and lines correspond to illumination with λ_{LED} = 460 nm and red colored ones to λ_{LED} = 810 nm. A good match is obtained when using the optical properties by Adachi,[38] whereas a poor agreement is found for the data from Palik.[39]

the data by Adachi.[38] For this data set, an equally good match of the calculated modulation amplitudes with the experimentally measured reflectivity profiles for the two samples with SiO$_2$ cover layer (1 μm and 3.5 μm thick) was obtained, as also shown in Figure 6 for the case of the data from Figure 4 (λ_{laser} = 3 μm). A much poorer agreement with the experimental results was obtained when using other data sets for the optical properties, as can be seen in Figure 6, where the values calculated with the data from Palik[39] are displayed.

Mode profile cross sections of light at $\lambda_{waveguide}$ = 1.55 μm propagating in amorphous waveguides was calculated with a 2D multilayer waveguide mode solver.[32] Table 1 included the optical constants at the wavelengths of interest for both types of calculations, taken from ref. [38].

Acknowledgements

Conflict of Interest

The authors declare no conflict of interest.

Data Availability Statement

Research data are not shared.

[1] V. R. Almeida, C. A. Barrios, R. R. Panepucci, M. Lipson, *Nature* **2004**, *431*, 1081.

[2] H. Wang, Y. Zhang, Y. He, Q. Zhu, L. Sun, Y. Su, *Adv. Opt. Mater.* **2018**, *7*, 1801191.

[3] M. J. A. De Dood, A. Polman, T. Zijlstra, E. W. J. M. Van Der Drift, *J. Appl. Phys.* **2002**, *92*, 649.

[4] M. A. Mohammed, J. Melskens, R. Stabile, F. Pagliano, C. Li, W. M. M. Kessels, O. Raz, *Adv. Opt. Mater.* **2020**, *8*, 1901680.

[5] P. L. Liu, R. Yen, N. Bloembergen, R. T. Hodgson, *Appl. Phys. Lett.* **1979**, *34*, 864.

[6] R. Yen, J. M. Liu, H. Kurz, N. Bloembergen, *Appl. Phys. A: Solids Surf.* **1982**, *27*, 153.

[7] A. L. Smirl, I. W. Boyd, T. F. Boggess, S. C. Moss, H. M. Van Driel, *J. Appl. Phys.* **1986**, *60*, 1169.

[8] Y. Izawa, Y. Izawa, Y. Setsuhara, M. Hashida, M. Fujita, R. Sasaki, H. Nagai, M. Yoshida, *Appl. Phys. Lett.* **2007**, *90*, 044107.

[9] Y. Izawa, S. Tokita, M. Fujita, M. Nakai, T. Norimatsu, Y. Izawa, *J. Appl. Phys.* **2009**, *105*, 064909.

[10] J. Bonse, K. W. Brzezinka, A. J. Meixner, *Appl. Surf. Sci.* **2004**, *221*, 215.

[11] J. Bonse, *Appl. Phys. A: Mater. Sci. Process.* **2006**, *84*, 63.

[12] C. Florian, D. Fischer, K. Freiberg, M. Duwe, M. Sahre, S. Schneider, A. Hertwig, J. Krüger, M. Rettenmayr, U. Beck, A. Undisz, J. Bonse, *Materials* **2021**, *14*, 1651.

[13] D. Puerto, M. Garcia-Lechuga, J. Hernandez-Rueda, A. Garcia-Leis, S. Sanchez-Cortes, J. Solis, J. Siegel, *Nanotechnology* **2016**, *27*, 265602.

[14] Y. Fuentes-Edfuf, M. Garcia-Lechuga, D. Puerto, C. Florian, A. Garcia-Leis, S. Sanchez-Cortes, J. Solis, J. Siegel, *Appl. Phys. Lett.* **2017**, *110*, 211602.

[15] Y. Fuentes-Edfuf, M. Garcia-Lechuga, D. Puerto, C. Florian, A. Garcia-Leis, S. Sanchez-Cortes, J. Solis, J. Siegel, *Sci. Rep.* **2017**, *7*, 4594.

[16] J. Colombier, A. Rudenko, E. Silaeva, H. Zhang, X. Sedao, E. Bévillon, S. Reynaud, C. Maurice, F. Pigeon, F. Garrelie, R. Stoian, *J. Rev. Res.* **2020**, *043080*, 1.

[17] F. Gesuele, J. J. J. Nivas, R. Fittipaldi, C. Altucci, R. Bruzzese, P. Maddalena, S. Amoruso, *Sci. Rep.* **2018**, *8*, 12498.

[18] K. Werner, V. Gruzdev, N. Talisa, K. Kafka, D. Austin, C. M. Liebig, E. Chowdhury, *Sci. Rep.* **2019**, *9*, 19993.

[19] J. Huang, L. Jiang, X. Li, Q. Wei, Z. Wang, B. Li, L. Huang, A. Wang, Z. Wang, M. Li, L. Qu, Y. Lu, *Adv. Opt. Mater.* **2019**, *7*, 1900706.

[20] D. H. Reitze, T. R. Zhang, W. M. Wood, M. C. Downer, *J. Opt. Soc. Am. B* **1990**, *7*, 84.

[21] K. Sokolowski-Tinten, D. von der Linde, *Phys. Rev. B* **2000**, *61*, 2643.

[22] V. P. Lipp, B. Rethfeld, M. E. Garcia, D. S. Ivanov, *Phys. Rev. B: Condens. Matter Mater. Phys.* **2014**, *90*, 245306.

[23] J. Bonse, S. Baudach, J. Krüger, W. Kautek, M. Lenzner, *Appl. Phys. A: Mater. Sci. Process.* **2002**, *74*, 19.

[24] E. Petrakakis, G. D. Tsibidis, E. Stratakis, *Phys. Rev. B* **2019**, *99*, 195201.

[25] F. F. Abraham, J. Q. Broughton, *Phys. Rev. Lett.* **1986**, *56*, 734.

[26] M. O. Thompson, J. W. Mayer, A. G. Cullis, H. C. Webber, N. G. Chew, J. M. Poate, D. C. Jacobson, *Phys. Rev. Lett.* **1983**, *50*, 896.

[27] M. von Allmen, A. Blatter, *Laser-Beam Interactions with Materials*, Springer, Berlin **1995**.

[28] X. Zhang, L. Zhang, S. Mironov, R. Xiao, L. Guo, T. Huang, *Appl. Phys. A: Mater. Sci. Process.* **2021**, *127*, 196.

[29] J. A. Yater, M. O. Thompson, *Phys. Rev. Lett.* **1989**, *63*, 2088.

[30] P. Kühler, D. Puerto, M. Mosbacher, P. Leiderer, F. J. G. de Abajo, J. Siegel, J. Solis, *Beilstein J. Nanotechnol.* **2013**, *4*, 501.

[31] J. Siegel, a. Schropp, J. Solis, C. N. Afonso, M. Wuttig, *Appl. Phys. Lett.* **2004**, *84*, 2250.

[32] *EIMS: 2-D Multilayer Waveguide Mode Solver, Variational Effective Index Approximation*, https://www.computational-photonics.eu/eims.html (accessed: January 2021).

[33] A. Das, A. Wang, O. Uteza, D. Grojo, *Opt. Express* **2020**, *28*, 26623.

[34] M. Garcia-Lechuga, D. Grojo, *Open Res. Eur.* **2021**, *1*, 7.

[35] J. M. Liu, *Opt. Lett.* **1982**, *7*, 196.

[36] M. Garcia-Lechuga, O. Uteza, N. Sanner, D. Grojo, *Opt. Lett.* **2020**, *45*, 952.

[37] M. Born, E. Wolf, A. B. Bhatia, P. C. Clemmow, D. Gabor, A. R. Stokes, A. M. Taylor, P. A. Wayman, W. L. Wilcock, *Principles of Optics*, Cambridge University Press, Cambridge **1999**.

[38] S. Adachi, in *Optical Constants of Crystalline and Amorphous Semiconductors*, Springer US, Boston, MA **1999**, pp. 18–32.

[39] E. D. Palik, *Handbook of Optical Constants of Solids*, Elsevier Inc., Amsterdam **2012**.